

VARIATIONAL METHOD FOR DENSE SYSTEMS

V. R. PANDHARIPANDE

Laboratory of Nuclear Studies, Cornell University, Ithaca, New York, U.S.A. and Tata Institute of Fundamental Research, Colaba, Bombay-5, India

Abstract. The variational method for calculating energy of quantum fluids, and its applications to the Bose liquid ${}^4\text{He}$, Fermi neutron gas, and liquid ${}^3\text{He}$ are discussed. The correlation functions are parameterized by their healing distance, and can depend on the states occupied by the correlated particles in the model wave function. They are calculated by constrained variation of lowest order contributions. The healing distance has a prescribed value in lowest order calculations, whereas it is sufficiently large in hopefully exact energy calculations. The direct many-body cluster diagrams are summed with successive approximations of an integral equation. The contribution of exchange diagrams is shown to decrease rapidly with the number of exchanges, and their sums are truncated after the energy has converged to within a few percent.

1. Introduction

An equilibrium mixture of hyperons, interacting through two-body potentials is the simplest model of dense matter, and its region of validity has been discussed by H. Bethe in his paper in this volume. (We will refer to it, hereafter, as Paper I.) In the non-relativistic limit of this model, the many-body Schrödinger equation

$$\left\{ \sum_i -\frac{\hbar^2}{2m_i} \nabla_i^2 + \frac{1}{2} \sum_{i < j} v_{ij} \right\} \Psi(1 \dots N) = E\Psi(1 \dots N) \quad (1)$$

should be solved for the variationally determined ground state composition to calculate the zero temperature energy as a function of density.

For practical reasons the form of the trial wavefunction used to solve (1) variationally is restricted to

$$\Psi(1 \dots N) = \prod_{i < j} f_{ij} \Phi(1 \dots N), \quad (2)$$

where Φ is a model fluid state wavefunction, and the correlation function f_{ij} is determined by minimizing the energy. We discuss two methods: in the first, the variation is constrained to enable us to make energy calculations in lowest order; in the second, the energy calculation is, we hope, exact and the variation is unconstrained.

Since there are many distinguishable hyperons of similar mass, hyperonic matter can be anywhere inbetween a Fermi and a Bose system when its composition is heterogeneous. At typical maximum densities in neutron stars (Baym *et al.*, 1971) the unit radius r_0 ,

$$\frac{4\pi}{3} r_0^3 \rho = 1 \quad (3)$$

almost equals r_c , the radius of the repulsive core in the n-n potential. In liquid ${}^3\text{He}$ and ${}^4\text{He}$ also the r_0 at equilibrium density is a few percent less than the He-He atomic

potential core radius. The binding energies of both types of liquid helium, Fermi ^3He and Bose ^4He are known, and have been extensively studied by variational methods with wavefunction (2) (as in Schiff and Verlet, 1967; and Murphy and Watts, 1970). These liquids form a suitable testing ground for many-body techniques used in hyperonic matter, and hence calculation of their energies is discussed in considerable detail. The He-He atomic potential core is very hard, and has $r^{-1.2}$ behavior at small r . It tends to induce much stronger correlations than the n-n soft core potential with its r^{-2} to r^{-3} behavior as pointed out in Paper I. Thus liquid He is probably too severe a test for the theoretical methods.

2. The Radial Distribution Function

The radial distribution function of a Bose fluid is defined as

$$g_{mn} = \Omega \int \prod_{i < j} f_{ij}^2 d\tau' / \int \prod_{i < j} f_{ij}^2 d\tau, \quad (4)$$

where $d\tau'$ omits integration over \mathbf{r}_{mn} , and Ω is the normalization volume. The subscripts denote coordinate variables of the functions, thus $g_{mn} = g(\mathbf{r}_{mn})$.

By convention we antisymmetrize only the left-hand side Ψ^* in calculations of expectation values for Fermi fluids. Thus initially the particles 1, 2, ... i respectively occupy plane wave states $\phi_1, \phi_2 \dots \phi_i$ with momenta $\mathbf{k}_1, \mathbf{k}_2 \dots \mathbf{k}_i$, and summation over particles is changed to summation over states. The radial distribution function for particles initially in states \mathbf{k}_m and \mathbf{k}_n can now be defined as

$$g(\mathbf{k}_m, \mathbf{k}_n) = \frac{\Omega \int \left(A \prod_i \phi_{q,i}^* \right) \left(\prod_{i < j} f_{ij}^2 \right) \left(\prod_i \phi_{i,i} \right) d\tau'}{\int \left(A \prod_i \phi_{q,i}^* \right) \left(\prod_{i < j} f_{ij}^2 \right) \left(\prod_i \phi_{i,i} \right) d\tau}, \quad (5)$$

where $\phi_{q,i}$ is the abbreviation of $\phi_q(\mathbf{r}_i)$. The true g is obviously

$$g(\mathbf{r}) = \frac{1}{N(N-1)} \sum_{i \neq j} g(\mathbf{k}_i, \mathbf{k}_j). \quad (6)$$

The f_{ij} approaches unity at large r_{ij} , and is small or zero at $r=0$. It is then convenient to substitute


$$f_{ij}^2 = 1 + F_{ij} \quad (7)$$


for all pairs other than mn in (4) or (5). The F_{ij} is a short-range function with absolute value generally less than unity, and products of $(1 + F_{ij})$ can be expanded in powers of F as follows:

$$\prod_{i < j} (1 + F_{ij}) = 1 + \sum_{i < j} F_{ij} + \prod_{i < j, k < l} \prod_{(ij \neq kl)} F_{ij} F_{kl} \dots \quad (8)$$


Integrals over various terms in (8) are represented by diagrams of the type shown in

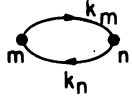
A. Bose Fluids : g_{mn} Diagrams

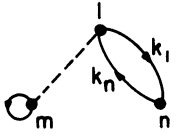
A.1  = $\Omega^N f_{mn}^2$

A.2  = $\Omega^{N-1} f_{mn}^2 \int F_{1m} F_{1n} d^3 r_1$

B. Fermi Fluids : $g(\vec{k}_m, \vec{k}_n)$ Diagrams

B.1  = $\Omega^N f_{mn}^2$

B.2  = $-\Omega^N f_{mn}^2 e^{i(\vec{k}_m - \vec{k}_n) \cdot \vec{r}_{mn}}$

B.3  = $-\Omega^{N-1} f_{mn}^2 \int F_{m1} F_{n1} e^{i(\vec{k}_n - \vec{k}_1) \cdot \vec{r}_{n1}} d^3 r_1$

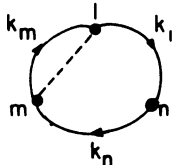
B.4  = $\Omega^{N-1} f_{mn}^2 \int F_{m1} e^{i(\vec{k}_m \cdot \vec{r}_{m1} + \vec{k}_n \cdot \vec{r}_{nm} + \vec{k}_1 \cdot \vec{r}_{1n})} d^3 r_{m1}$

Fig. 1. Radial distribution function diagrams.

Figure 1. The points in these diagrams represent the particle coordinates, broken lines represent F functions, and numerator diagrams must always contain points m and n with f_{mn}^2 . In Fermi fluid diagrams the full line k_q entering r_i represents the final state ϕ_q occupied by the particle in the left-hand side Ψ^* . The lines $k_1 \dots k_i$ must originate from points $1 \dots i$ respectively by our convention. The g_{mn} is simply the sum of all irreducible numerator diagrams divided by Ω^N (Pandharipande and Bethe, 1972).

3. The Energy

The potential, and the part of the kinetic energy obtained by collecting terms in which

∇^2 operates on a single f_{ij} can be included in an effective potential V_{ij} , and 'potential energy' W defined as

$$V_{ij} = v_{ij} - \frac{\hbar^2 \nabla^2 f_{ij}}{m f_{ij}}, \quad (9)$$

$$W = \frac{1}{2\Omega} \sum_{i,j} \int V_{ij} g_{ij} d^3 r_{ij}. \quad (10)$$

The ∇_i^2 operating on f_{ij} and f_{ik} gives additional kinetic energy U ,

$$U = - \frac{1}{\Omega^2} \frac{\hbar^2}{2m} \sum_{i,j,k} \int g_3(r_{ij}, r_{ik}) \frac{\nabla_i f_{ij} \cdot \nabla_i f_{ik}}{f_{ij} f_{ik}} d^3 r_{ij} d^3 r_{ik}, \quad (11)$$

where $g_3(r_{ij}, r_{ik})$ is a three-particle distribution function defined analogous to g_{ij} . The total energy of the Bose fluid is simply

$$E = W + U. \quad (12)$$

In Fermi fluids the terms in which ∇^2 operates on Φ give exactly the Fermi gas energy T ,

$$T = \sum_i \frac{\hbar^2}{2m_i} k_i^2, \quad (13)$$

because Φ is an eigenfunction of ∇^2 . A term W_F is obtained in addition to W from $(\nabla_i^2 + \nabla_j^2)$ operating on ϕ_i or ϕ_j , and f_{ij} , that is,

$$W_F = - \frac{1}{\Omega} \sum_{k_i, k_j} \frac{\hbar^2}{m_{ij}} \frac{\nabla f_{ij} \cdot \nabla \phi_{ij}}{f_{ij} \phi_{ij}} g(\mathbf{k}_i, \mathbf{k}_j) d^3 r_{ij}, \quad (14)$$

where m_{ij} is the reduced mass for particles i and j , and the relative model wave function is

$$\phi_{ij} = \exp[i \frac{1}{2} (\mathbf{k}_i - \mathbf{k}_j) \cdot \mathbf{r}_{ij}]. \quad (15)$$

Similarly the operation of ∇_i^2 on f_{ij} and ϕ_{ik} gives another term

$$U_F = \frac{-1}{\Omega^2} \sum_{k_i, k_j, k_k} \frac{\hbar^2}{2m_i} g_3(\mathbf{k}_i, \mathbf{k}_j, \mathbf{k}_k, \mathbf{r}_{ij}, \mathbf{r}_{ik}) \frac{\nabla_i f_{ij} \cdot \nabla_i \phi_{ik}}{f_{ij} \phi_{ik}} d^3 r_{ij} d^3 r_{ik}, \quad (16)$$

and the total energy is

$$E = T + W + W_F + U + U_F. \quad (17)$$

The terms W and W_F can be combined by redefining the effective potential (9) for Fermi systems as

$$V_F(\mathbf{k}_i, \mathbf{k}_j, \mathbf{r}_{ij}) = v(\mathbf{r}_{ij}) - \frac{\hbar^2}{m_{ij}} \left\{ \frac{\nabla^2 f_{ij}}{f_{ij}} + 2 \frac{\nabla f_{ij} \cdot \nabla \phi_{ij}}{f_{ij} \phi_{ij}} \right\}. \quad (18)$$

4. Constrained Variation

Most of the results presented in Paper I are obtained with this simple method. The physical assumption here is that the contribution of farther neighbors of a particle i to the instantaneous potential $\sum_j v_{ij}$ seen by i should mostly be included in the average field of which ϕ_i is an eigenfunction. Hence distant neighbors should not be strongly correlated, and the effect of their correlation on the energy should be small. If this effect is neglected one can work with correlation functions satisfying the conditions

$$\text{if } f_{ij} \neq 1 \text{ then all } f_{ik} = 1 \tag{19}$$

when ij are nearest neighbors. It is difficult to handle (19) because it couples various f_{ij} . In practice (19) is approximated as a healing constraint on a single f_{ij} as a function of r_{ij} as follows (Pandharipande, 1971):

$$f_{ij}(|r_{ij}| > d) = 1, \text{ and } (\partial f_{ij}/\partial r_{ij})(|r_{ij}| = d) = 0. \tag{20}$$

The healing distance d is chosen such that, on the average, there is only one particle within a distance d of an average particle. With this constraint correlations are at times allowed between second and more distant neighbors, and at times even the first neighbors are treated as uncorrelated. We hope that these effects cancel.

All higher order direct diagrams are zero if (19) is valid, and we will show that higher order exchange diagrams like B.4 of Figure 1, which can contribute even when (19) is valid, are small. Thus the energy can be calculated with only the two-body term in the cluster expansion, which is

$$\frac{E}{N} = \frac{1}{2} \rho \int \left(v - \frac{\hbar^2 \nabla^2 f}{m f} \right) f^2 d^3r \tag{21}$$

for Bose fluids. (We omit subscripts wherever unnecessary.) Before minimizing E with respect to variations in f , the part of v that contributes to the average field and hence does not induce correlations, must be subtracted from (21). The constraint (20) gives for this part denoted by $\lambda(r)$,

$$\lambda(|r| > d) = v(r), \tag{22}$$

and we assume $\lambda(|r| < d)$ to be a constant λ_0 to be determined from (20). The equation

$$\delta \int_0^d \left\{ -\frac{\hbar^2}{m} f \nabla^2 f + v f^2 - \lambda_0 f^2 \right\} d^3r = 0 \tag{23}$$

gives directly the two body Schrödinger equation for $r < d$

$$-\frac{\hbar^2}{m} \nabla^2 f + v f = \lambda_0 f \tag{24}$$

and λ_0 can be obtained from the boundary condition (20). The effective potential

V_{ij} is clearly

$$\begin{aligned} V_{ij}(|r_{ij}| < d) &= \lambda_0 \\ V_{ij}(|r_{ij}| > d) &= v_{ij}(r_{ij}). \end{aligned} \quad (25)$$

The f and λ_0 are functions of d , which is determined from

$$\rho \int_0^d f^2 d^3r = 1, \quad (26)$$

where the left-hand side is simply the average number of particles within d as calculated in lowest order. The two Equations (24) and (26) are solved simultaneously.

In Fermi fluids let us first consider pairs of distinguishable fermions like those of spin up and spin down particles of a baryon type, or of two different baryons of any spin direction. Such pairs are not exchanged in the antisymmetrization of the wave function. If the two particles are in states \mathbf{k}_i and \mathbf{k}_j , the lowest order contribution of their interaction to the potential energy ($W + W_F$) is given by Equations (10) and (18) as

$$(W + W_F)_{ij} = \frac{1}{\Omega} \int \phi_{ij}^2 f^{ij2} \left\{ v - \frac{\hbar^2}{m} \left[\frac{\nabla^2 f^{ij}}{f^{ij}} + 2 \frac{\nabla f^{ij} \cdot \nabla \phi_{ij}}{f^{ij} \phi_{ij}} \right] \right\} d^3r, \quad (27)$$

where f^{ij} is the correlation function for particles in model states $\mathbf{k}_i, \mathbf{k}_j$, and ϕ_{ij} is given by (15). Since

$$\frac{\nabla^2 \phi_{ij}}{\phi_{ij}} = - \left[\frac{1}{2} (k_i - k_j) \right]^2 \equiv -k^2, \quad (28)$$

we can write (27) as

$$(W + W_F)_{ij} = \frac{1}{\Omega} \int \psi^* \left(v - \frac{\hbar^2}{m} k^2 - \frac{\hbar^2}{m} \nabla^2 \right) \psi d^3r, \quad (29)$$

with

$$\psi = f^{ij} \phi_{ij}, \quad (30)$$

and the constraint (19) as

$$\frac{\nabla \psi}{\psi}(\mathbf{r}, |r| = d) = \frac{\nabla \phi_{ij}}{\phi_{ij}}(\mathbf{r}, |r| = d). \quad (31)$$

It is convenient to decompose ϕ_{ij} and ψ in partial waves

$$\begin{aligned} \phi_{ij}(r) &= \sum_{l,m} kr j_l(kr) P_l^m(\theta, \phi) \\ \psi(r) &= \sum_{l,m} kr u_l(r) P_l^m(\theta, \phi). \end{aligned} \quad (32)$$

If v is spherically symmetric the various l states are not coupled, and the contribution of each can be minimized separately following the procedure described for the Bose

fluids. The equation for u_l is

$$-\frac{\hbar^2}{m} \frac{\partial u_l^2}{\partial r^2} + \frac{l(l+1)}{r^2} u_l + v u_l = \left(\frac{\hbar^2}{m} k^2 + \lambda_0^l \right) u_l \tag{33}$$

and λ_0^l is determined from the boundary condition

$$\frac{1}{u_l(d)} \frac{\partial u_l(d)}{\partial r} = \frac{1}{j_l(kd)} \frac{\partial j_l(kd)}{\partial r} \tag{34}$$

Both the correlation function f and the effective interaction V_F depend upon k and l , and may be written as

$$f_{ij} = \sum_l f^l(k, r) P_{ij}^l \tag{35}$$

$$V_{Fij} = (r < d) = \sum_l \lambda_0^l(k) P_{ij}^l \tag{36}$$

$$V_{Fij} = (r > d) = v_{ij}, \tag{37}$$

where the projection operators P_{ij}^l operate only on the model wave function $\phi_{q,i} \phi_{p,j}$ by definition.

The same procedure can be followed in calculating the contribution of interaction between parallel spin fermions of the same type in states \mathbf{k}_i and \mathbf{k}_j . Adding the exchange contribution to (29) gives

$$(W + W_F)_{ij\uparrow\uparrow} = \frac{1}{\Omega} \int [\psi^*(\mathbf{r}) - \psi^*(-\mathbf{r})] \left(v - \frac{\hbar^2}{m} k^2 - \frac{\hbar^2}{m} \nabla^2 \right) \psi(\mathbf{r}) d^3r, \tag{38}$$

and on substituting the partial wave expansion (32) in (38) the even l -state contributions cancel, and those of odd states are doubled. The variational calculation of f_{ij} and V_{Fij} is unaffected because (33) is obtained by individually minimizing the contribution of each partial wave. The d is given by

$$\frac{1}{\Omega^2 N} \sum_{ij} \langle \phi_i \phi_j - \phi_j \phi_i \delta_{\uparrow\uparrow} | \left\{ \sum_l f^l(\mathbf{k}, \mathbf{r}) P^l \right\} \tilde{O}(d) | \phi_i \phi_j \rangle = 1, \tag{39}$$

where $\tilde{O}(d) = 1$ for $r < d$ and zero otherwise. Equations (33), (34) and (39) are solved simultaneously by iteration.

The above method is simple enough to study complex systems like dense hyperonic matter, and still sufficiently general to treat the small differences in baryon-baryon interactions, interactions in different angular momentum states, and baryon masses. It is also possible to generalize it to treat non-central forces, particularly the strong tensor force in the neutron-proton interaction (Pandharipande, 1972; Pandharipande and Garde, 1972).

However, there are approximations in this model justified by purely physical arguments. In particular, the healing distance d is obtained from a lowest order calculation

of the number of particles within d . This may not be valid when $d \gg r_0$, where r_0 equals d in uncorrelated systems. In neutron star matter $d \sim 1.2 r_0$ whereas in liquid helium $d \sim 1.4 r_0$, because helium atomic cores are much harder than the baryonic cores. The variational property $E \geq \text{true } E_0$ is lost due to the lowest order calculation of E . In subsequent sections we describe what we hope are exact calculations of E with sufficiently large values of d so that the effects of the constraint are negligible. A comparison of the two calculations should ascertain the region of validity of the first.

5. Integral Equation for Summing Direct Diagrams

Some of the diagrams that contribute to the radial distribution function in a Bose system are shown in Figure 2. A sum over all particles labeled by numbers 1, 2, ... is implied, and it simply gives a density ρ with factors to account for double counting. Thus the contribution of diagram E.2 of Figure 2 is

$$f_{mn}^2 \rho \int F_{1m} F_{1n} d^3 r_1 \equiv f_{mn}^2 S_{mn}. \quad (40)$$

The functions F and S are shown in Figure 3 for a typical f with $d = 2 r_0$, in liquid ^4He near equilibrium density. Since the magnitude of S is larger than that of F , and they are of opposite sign, the contribution of diagram E.3

$$= f_{mn}^2 \rho \int F_{1m} S_{1n} d^3 r_1 \quad (41)$$

is larger than that of (40). It can be easily seen that E.4 contributes more than E.3, etc. The diagrams E.2, E.3 ... are called single chains, and in dense fluids their contribution does not decrease with the number of particles in the chain.

The contribution of diagram E.5

$$= f_{mn}^2 \rho \int F_{m1} F_{n1} S_{n1} d^3 r_1, \quad (42)$$

and is of the same order as that of E.2 because $S \gtrsim 1$ in the range of F . Thus diagrams of type E.5–7 in which additional chains are added to connect two particles in a chain are also of the same order as those of single chains. Diagrams in which any two points of a chain may be connected by many chains are called hypernetted chains (HNC), and E.8 is a typical HNC diagram. No two chains, or subchains, are connected by an F .

The simplest diagram in which two chains connecting m and n are connected by an F is E.9. Its contribution \mathcal{S} is small (Figure 6), particularly in the region where f_{mn}^2 is appreciable, because all four particles have to be within the range of F . One would thus expect contributions of diagrams like E.10 involving E.9 as a subdiagram to be small.

Van Leeuwen *et al.* (1959) have shown that the sum of all diagrams in the Bose case

is given by the consistent solution of

$$\ln \left\{ \frac{g_{mn}}{f_{mn}^2 \exp(E_{mn})} \right\} = \varrho \int \left\{ g_{m1} - 1 - \ln \left[\frac{g_{m1}}{f_{m1}^2 \exp(E_{m1})} \right] \right\} (g_{n1} - 1) d^3r_1. \tag{43}$$

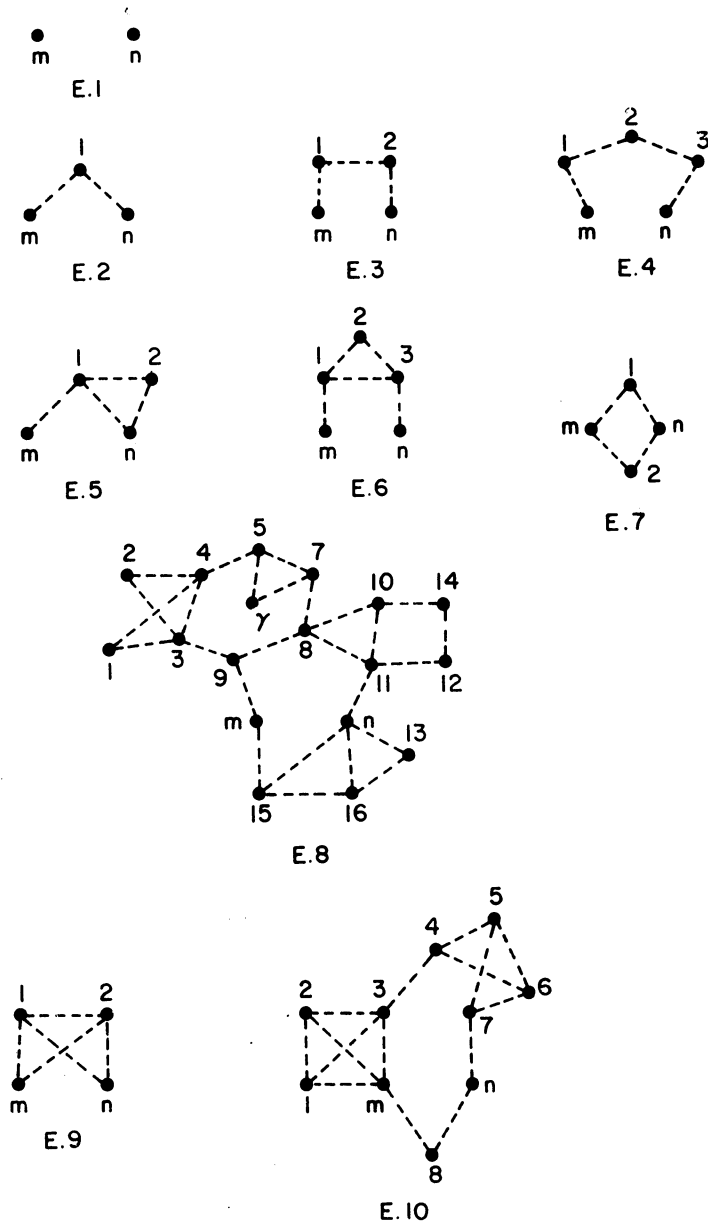


Fig. 2. Irreducible diagrams that contribute to Bose $g(r)$.

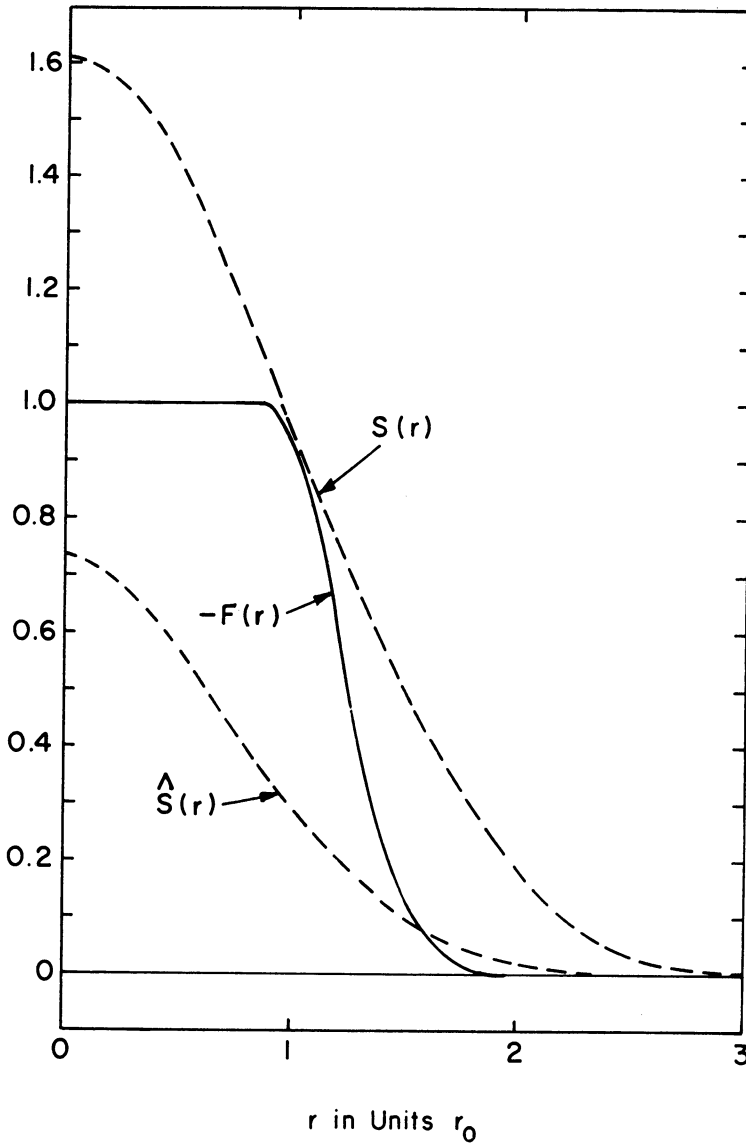


Fig. 3. The functions, F , S , and S in liquid ${}^4\text{He}$ at $\rho = 0.35$ atoms σ^{-3} and $d = 2 r_0$ with the Lennard-Jones potential.

If E_{mn} is set equal to zero one obtains the sum of all HNC diagrams. When $E_{mn} = \hat{S}_{mn}$ the equation sums all HNC diagrams plus the diagram E.9 and the HNC's formed with E.9 as an element. We call this approximation HNC/4. The difference between HNC and HNC/4 is rather small (Figure 6) and hence more complicated diagrams in which many particles have to be simultaneously correlated with all others can be neglected.

It is clear that summing all HNC diagrams connecting ij , jk , and ki gives for the three-boson distribution function

$$g_3(\mathbf{r}_{ij}, \mathbf{r}_{ik}) = g_{ij}g_{jk}g_{ki}. \tag{44}$$

We use (44) to obtain g_3 in both HNC and HNC/4 approximations.

6. Exchange Diagrams

The state dependence of the correlation function, that is equations (35) to (37), and that of the potential in the case of neutron matter, makes exact higher order cluster calculations in Fermi fluids very complex. We note that the short range part of the n - n potential, which is mainly responsible for the correlations, is similar in all states (Paper I). The l and k dependence of f is also not too strong for the neutron case, and hence higher order Fermi fluid calculations are simplified considerably by neglecting the differences between $f(\mathbf{k}_m, \mathbf{k}_n)$ and $V_F(\mathbf{k}_m, \mathbf{k}_n)$ in all but the lowest order two-body clusters.

The sum of direct $g(k_m, k_n)$ diagrams can be easily calculated by the integral Equations (43) when the F^{ij} are approximated by an average F ,

$$F = \frac{1}{N^2} \sum_{ij} f^{ij^2} - 1 \equiv f^2 - 1. \tag{45}$$

Let g_B be the solution of (43) with the average f , and let

$$h = g_B/f^2. \tag{46}$$

Then the approximate contribution of all direct diagrams to $g(k_m, k_n)_D$ is

$$g_B(\mathbf{k}_m, \mathbf{k}_n)_D = (f^{mn})^2 h. \tag{47}$$

Figure 4 shows diagrams in which only particles in states k_m and k_n are exchanged, all f^{ij} other than f^{mn} are approximated by the average f , and the sums over states other than k_m and k_n are performed. As discussed previously, all HNC (or better, HNC/4), diagrams connecting m and n must be summed to any number of particles, and the crossed line of diagram G.4 denotes such a sum. The contribution of G.4 is obviously

$$g_B(\mathbf{k}_m, \mathbf{k}_n)_{ex} = - \exp[i(\mathbf{k}_m - \mathbf{k}_n) \cdot \mathbf{r}] g_B(\mathbf{k}_m, \mathbf{k}_n)_D. \tag{48}$$

Exchange of a particle in state m or n with another particle gives diagrams of type H.1 in Figure 5, and their average contribution is evaluated by summing over \mathbf{k}_m and \mathbf{k}_n . The sum of all direct diagrams connecting m and l is represented by the double broken line, and equals $(g_B - 1)$. Sum over exchanges k_1 and k_n gives the square of The Slater function $S(k_F r)$ [not to be confused with S of (40)],

$$\begin{aligned}
 S(k_F r) &= \frac{1}{N} \sum_i e^{i k_i \cdot r} \\
 &= \frac{3}{k_F^3 r^3} [\sin(k_F r) - k_F r \cos(k_F r)].
 \end{aligned}
 \tag{49}$$

The sum of diagrams with and without F_{1n} gives f_{1n}^2 which is converted to g_{B1n} by summing all chains connecting 1 and n . Thus the double full line $1n$ denotes

$$F_{ex}(r_{1n}) = \frac{1}{2} g_B S(k_F r_{1n})^2,
 \tag{50}$$

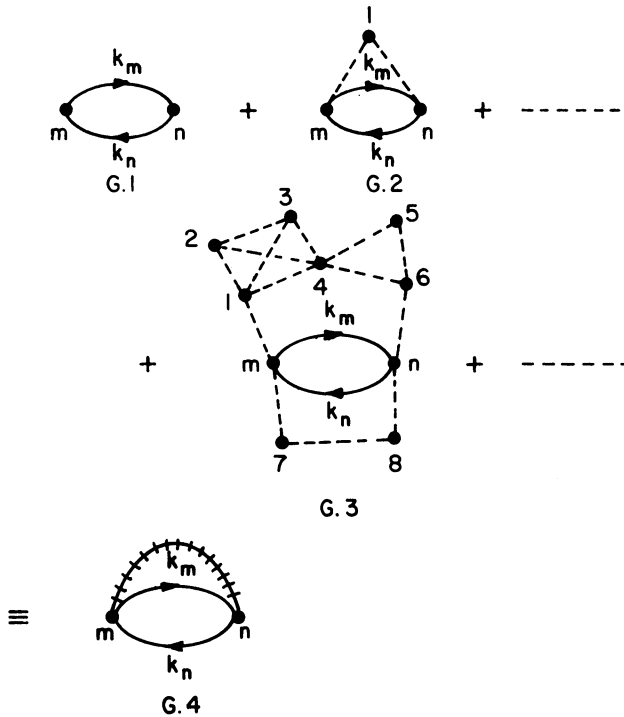


Fig. 4. Fermi $g(k_m, k_n)$ diagrams with one exchange.

where the factor $1/2$ comes from requiring that the spins of particles 1 and n must be parallel. The

$$\begin{aligned}
 g_{H.1}(\text{average}) &= -2g_B \rho \int (g_{Bm1} - 1) F_{ex}(r_{1n}) d^3 r_1, \\
 &\equiv f^2 h_1
 \end{aligned}
 \tag{51}$$

exchanges of m giving the factor 2.

Exchanging m and 1 in H.1 gives the three-particle exchange diagrams $g_{H.1 ex}$. Full

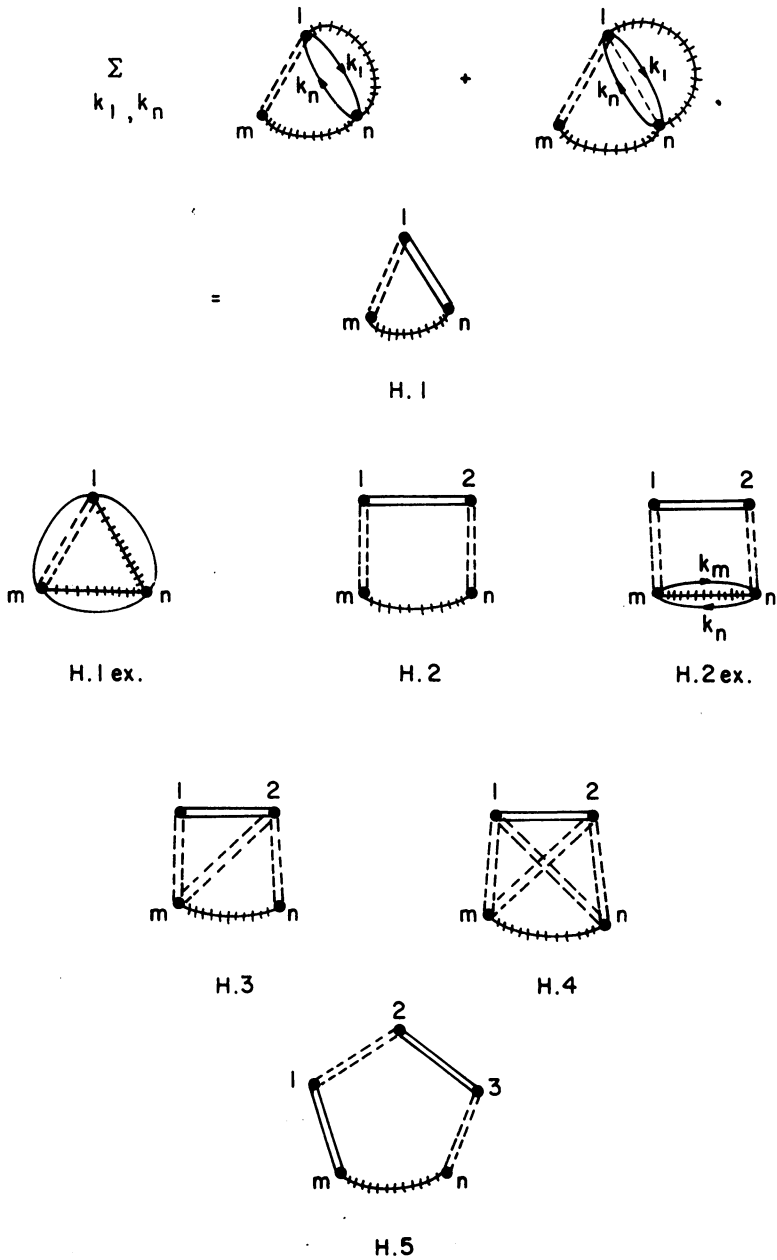


Fig 5. Fermi g diagrams with exchanges in the chains.

lines in this diagram represent the Slater functions, and their contributions

$$g_{H.1 \text{ ex}}(\text{average}) = 2S(k_F r_{mn}) g_B \varrho \int (g_{Bm1} - 1) S(k_F r_{m1}) g_{Bn1} \times \\ \times S(k_F r_{n1}) d^3 r_1 \equiv f^2 h_{1 \text{ ex}} \tag{52}$$

cancels $g_{H.1}$ at small r_{mu} when m and n have parallel spins.

In this notation it is quite simple to write the contributions of more complicated exchange diagrams; that of H.2 in Figure 5 is, for example,

$$g_{H.2}(\mathbf{k}_m, \mathbf{k}_n) = -g_B(\mathbf{k}_m, \mathbf{k}_n)_D \varrho^2 \int (g_{Bn1} - 1) F_{\text{ex}}(r_{12}) (g_{Bn2} - 1) \times \\ \times d^3 r_1 d^2 r_2 \equiv h_2 f^{mn^2}. \tag{53}$$

Figure 6 shows the functions $g_{2\text{-body}} (= f^2)$, $\Delta g_{\text{HNC}} (= g_{\text{BHNC}} - f^2)$, $\Delta g (= \Delta g_{\text{BHNC}/4} - \Delta g_{\text{BHNC}})$, $g_{H.1}$, and $g_{H.2}$ (average) in liquid ^3He at experimental equilibrium density.

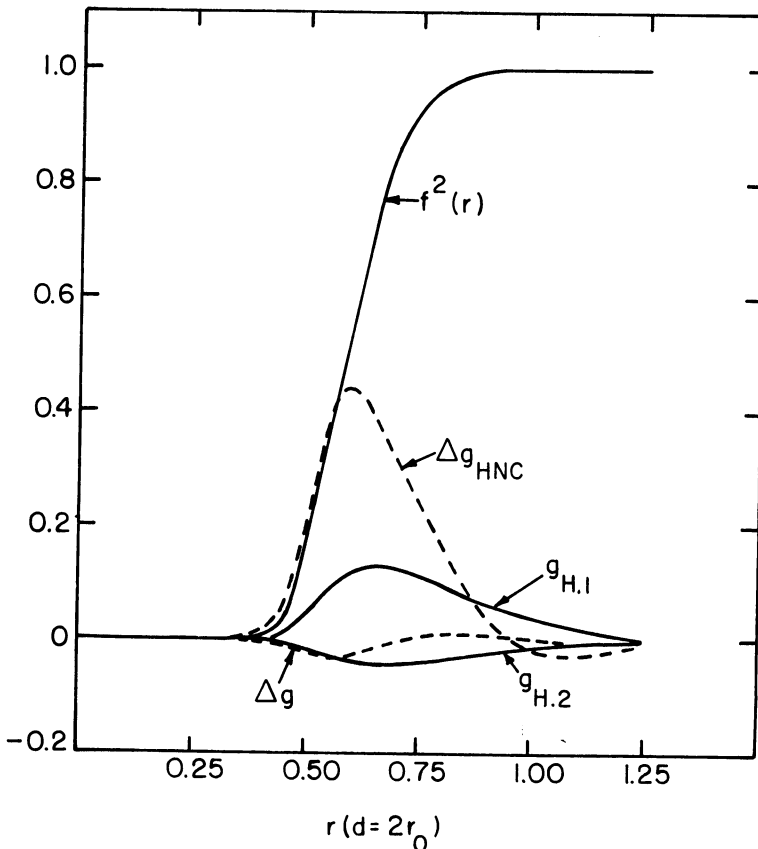


Fig. 6. Contributions to the radial distribution function in liquid ^3He at $\varrho = 0.277$ atoms σ^{-3} and $d = 2 r_0$ from various classes of diagrams.

The F_{ex} is a rather small function because g is small where $S(k_F r)$ is unity and vice versa. Hence the diagrams with exchanges in the chains give a small contribution. We neglect diagram H.4 because its contribution should be much smaller than Δg which itself is small. The contributions of H.1, H.2, and H.3 should be treated together because all these diagrams involve only one F . The maximum contribution of H.5 containing two F_{ex} is only 0.016 at $r \sim 0.6 d$. Since H.5 is expected to be the largest of all diagrams with two F_{ex} , all more complicated exchange diagrams can be safely neglected.

The three-particle distribution function $g_3(\mathbf{k}_i, \mathbf{k}_j, \mathbf{k}_k, \mathbf{r}_{ij}, \mathbf{r}_{ik})$ for various exchanges between i, j and k can be easily expressed in terms of the functions h with the superposition approximation (44).

7. Conclusions

The energy of liquid ^4He , as calculated in the HNC/4 approximation, is shown in Figure 7 as a function of (d/r_0) . It is very insensitive to d in the neighborhood of $2 r_0$. Hence most of our calculations are carried out with $d=2 r_0$.

Table I compares energies of a pure neutron gas as calculated with the Reid potential (Pandharipande, 1971) in the HNC and HNC/4 approximations. The maximum

TABLE I
The $E(\rho)$ for neutron gas with the Reid potential

ρ (n fm ⁻³)	(E/n) in MeV	
	HNC	HNC/4
0.2	19.77	19.77
0.6	77.08	77.00
1.0	170.5	169.7
1.4	293.5	292.0
1.8	440.4	438.8
2.2	607.3	606.8
2.6	790.5	793.4
3.0	987.9	997.4
3.4	1197.5	1217.4
3.8	1417.8	1452.4
4.2	1647.3	1701.6
4.6	1885.3	1963.4
5.0	2130.6	2237.6

difference is $\sim 5\%$, and we hope that the effect of more complicated direct diagrams will be $\ll 5\%$. The energy change on the inclusion of the exchange diagram H.5 is only $\sim 1-2\%$. When $d=2 r_0$ the higher order clusters contribute a substantial fraction $\sim 50\%$ of the total energy as shown in Table II.

Results of the constrained variational calculation in lowest order, and of (we hope) exact energy calculations with unconstrained d are compared in Figures 8, 9, and 10. The two calculations agree very well in neutron matter, whereas the simple lowest

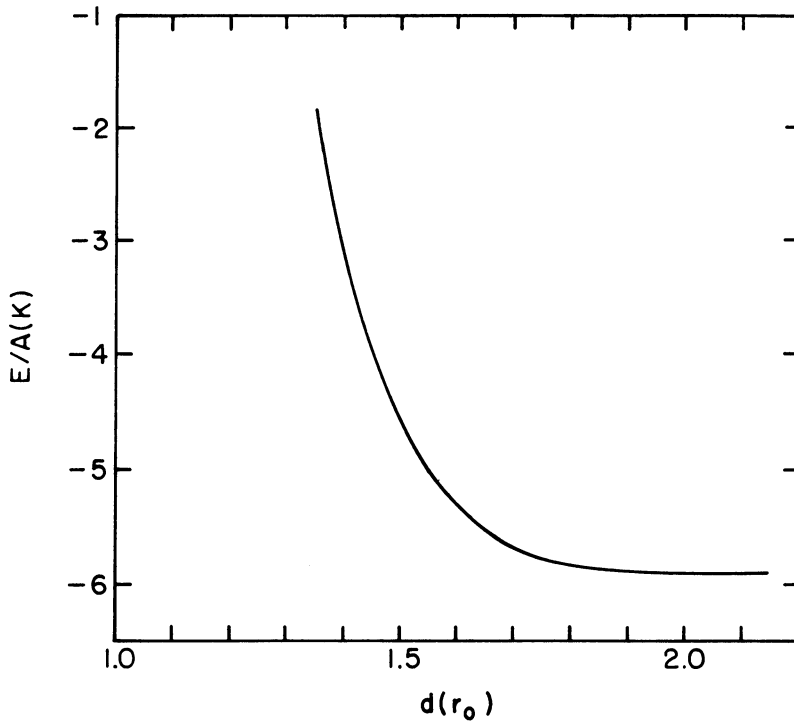


Fig. 7. Variation of energy with d in liquid ${}^4\text{He}$ at $\rho = 0.35$ atoms σ^{-3} with Lennard-Jones potential.

TABLE II
The contributions to $E(\rho)$ in neutron gas with Reid potential

ρ ($N \text{ fm}^{-3}$)	T	HNC/4 contribution to energy in MeV neutron					E
		$(W + W_F)_{\text{L.O.}}$	$\Delta(W + W_F)_{\text{H.O.}}$	U	U_F	All H.O.	
0.2	40.7	-21.4	-0.6	0.6	0.5	0.5	19.77
0.6	84.6	-26.4	+0.6	11.3	6.9	18.7	77.00
1.0	119	-11.0	16.3	30.8	14.6	61.8	169.7
1.4	149	21.9	44.5	54.5	22.4	121	292.0
1.8	176	70.6	82.5	79.8	29.9	192	438.8
2.2	201	133	129	106	37.3	272	606.8
2.6	225	209	182	133	44.6	359	793.4
3.0	248	296	241	160	51.8	453	997.4
3.4	269	394	307	189	59.0	554	1217.4
3.8	290	502	378	216	66.2	661	1452.4
4.2	310	618	456	246	73.5	773	1701.6
4.6	329	743	538	273	80.8	892	1963.4
5.0	348	875	625	300	89.9	1015	2237.6

order calculation overestimates the binding energies and equilibrium densities of liquid ^3He and ^4He by $\sim 20\%$.

Table III shows the total energy, the lowest order, and higher order contributions to it at $d/r_0 = 1.2, 1.6,$ and 2.0 . The total energy is much less sensitive to d than its decomposition into lowest and higher cluster contributions. The higher order contributions increase by a factor of $1.5\text{--}3.0$ whereas the total energy decreases only by $10\text{--}15\%$ and d is increased from 1.2 to $2 r_0$.

The $d = 1.2 r_0$ in lowest order calculations. Thus correlations with $d = 1.2 r_0$ are mainly two-body correlations because of the average there is only one neutron within

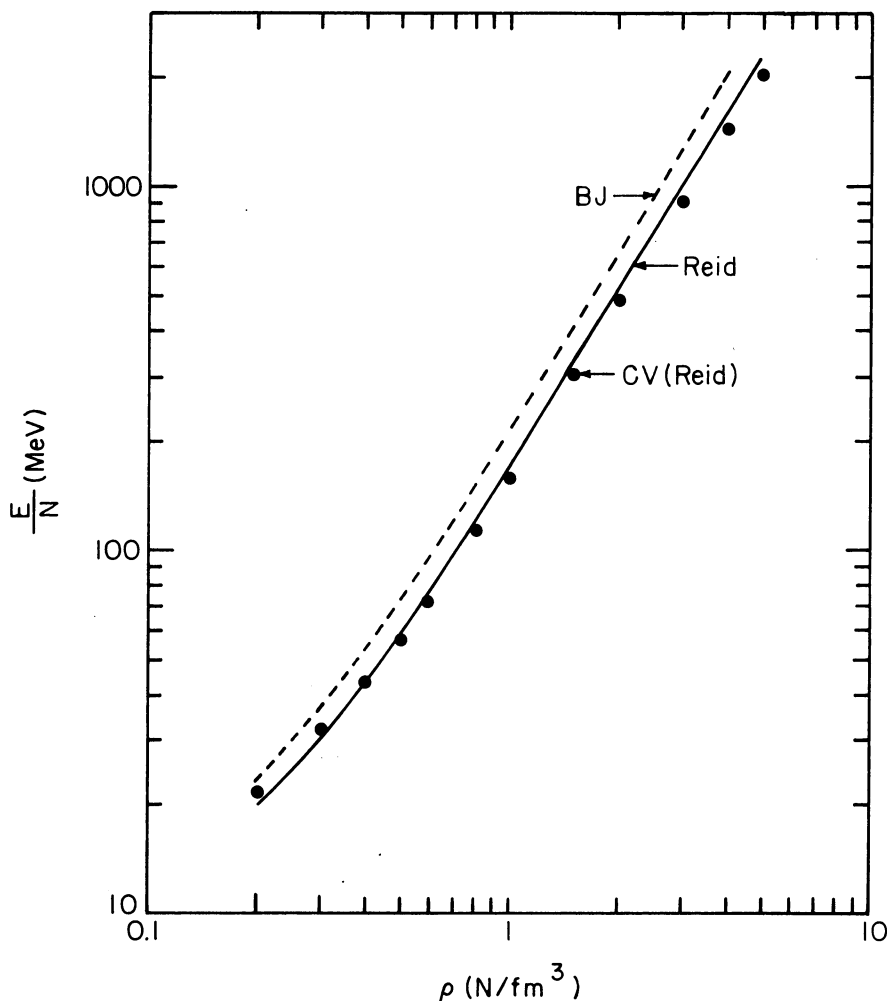


Fig. 8. Neutron gas energy: The full and broken lines give the results of 'exact' energy calculation with Reid and the modified Reid potentials, and the points show results of lowest order constrained variation (from Pandharipande, 1971).

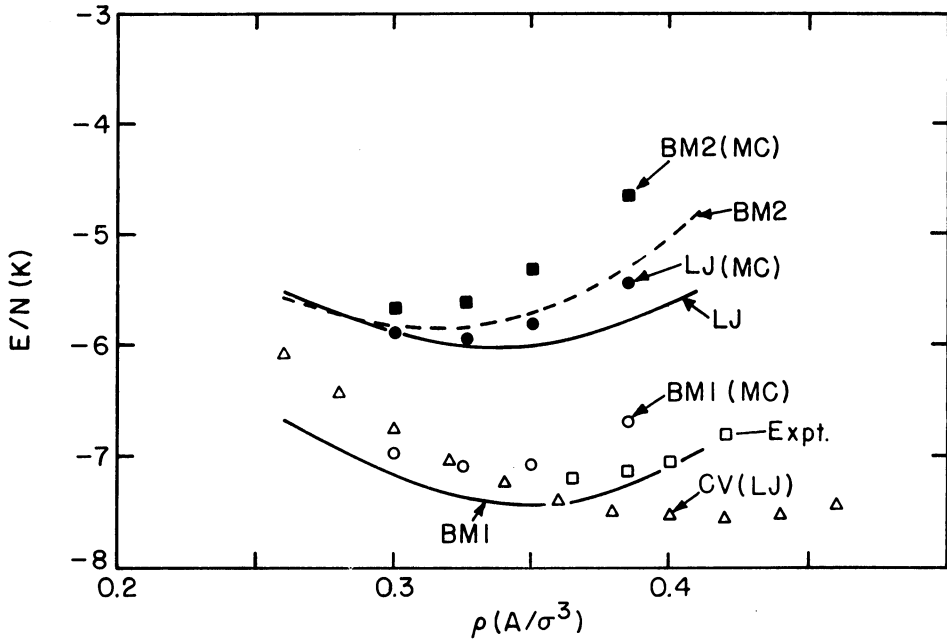


Fig. 9. Energy of liquid ^4He : The potentials and the Monte Carlo results are from Murphy and Watts (1970). The curves give results of present calculations, and those of lowest order constrained variation are from Pandharipande (1971).

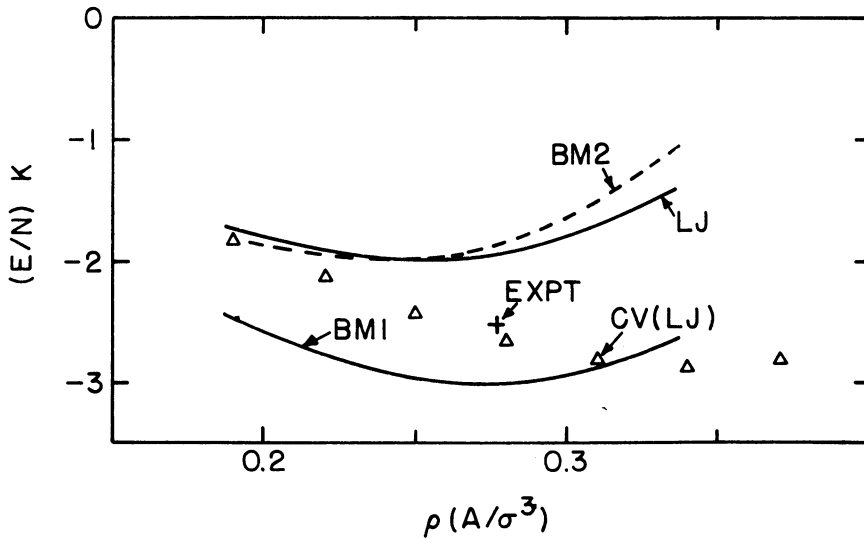


Fig. 10. Energy of liquid ^3He with various potentials.

TABLE III

The neutron-gas energy with Reid potential at various values of d

ρ ($N \text{ fm}^{-3}$)	(E/N) MeV	1.2	1.6	2.0
1.0	Total	204.4	177.3	169.7
	L.O.	156.3	123.7	108.0
	H.O.	38.1	53.6	61.7
3.0	Total	1174.0	1037.7	997.4
	L.O.	982.5	710.6	544.3
	H.O.	191.5	327.1	453.1
5.0	Total	2467.7	2266.0	2237.6
	L.O.	2117.5	1595.0	1223.0
	H.O.	350.2	671.0	1014.6

correlation volume of any given neutron. The small higher order cluster contributions at $d = 1.2 r_0$ come from events in which two (or more) neutrons come within the correlation volume of a neutron. In lowest order calculations these are neglected assuming that they cancel events in which the neutron can have a larger correlation volume because there is nothing within $1.2 r_0$ of it. The actual higher order calculations show that the occurrence of two or more neutrons in the correlation volume gives a somewhat greater contribution than the occurrence of none.

Our main result is the justification, for neutron matter, of the constrained lowest order calculation, to 5% or better, by the more exact calculation of higher order clusters. In Paper I the constrained lowest order method was used.

This work was supported, in part, by the National Science Foundation.

References

- Baym, G., Pethick, C., and Sutherland, P.: 1971, *Astrophys. J.* **170**, 299.
 van Leeuwen, J. M. J., Geoneveld, J., and de Boer, J.: 1959, *Physica* **25**, 792.
 Murphy, R. D. and Watts, R. O.: 1970, *J. Low Temperature Phys.* **2**, 507.
 Pandharipande, V. R.: 1971, *Nucl. Phys.* **A178**, 123.
 Pandharipande, V. R.: 1972, *Nucl. Phys.* **A181**, 33.
 Pandharipande, V. R. and Bethe, H. A.: 1972 (to be published).
 Pandharipande, V. R. and Garde, V. K.: 1972, *Phys. Letters* **39B**, 608.
 Schiff, D. and Verlet, L.: 1967, *Phys. Rev.* **160**, 208.